RSC Advances

PAPER

View Article Online
View Journal | View Issue



Cite this: *RSC Adv.*, 2020, **10**, 39875

# *Operando* soft X-ray absorption spectroscopic study on microporous carbon-supported sulfur cathodes†

Yao Xiao,[a] Kentaro Yamamoto,*[a] Yukiko Matsui,[b] Toshiki Watanabe,[a] Koji Nakanishi,[a] Tomoki Uchiyama,[a] Shoso Shingubara,[c] Masashi Ishikawa,[b] Masayoshi Watanabe[d] and Yoshiharu Uchimoto[a]

Sulfur is a promising material for next-generation cathodes, owing to its high energy and low cost. However, sulfur cathodes have the disadvantage of serious cyclability issues due to the dissolution of polysulfides that form as intermediate products during discharge/charge cycling. Filling sulfur into the micropores of porous carbon is an effective method to suppress its dissolution. Although microporous carbon-supported sulfur cathodes show an electrochemical behavior different from that of the conventional sulfur ones, the corresponding reaction mechanism is not clearly understood. In this study, we focused on clarifying the reaction mechanism of microporous carbon-supported sulfur cathodes by *operando* soft X-ray absorption spectroscopy. In the microporous carbon support, sulfur was present as smaller fragments compared to conventional sulfur. During the first discharge process, the sulfur species in the microporous carbon were initially reduced to $S_6^{2-}$ and $S_2^{2-}$ and then to $Li_2S$. The $S_6^{2-}$ and $S_2^{2-}$ species were observed first, with $S_2^{2-}$ being the main polysulfide species during the discharge process, while $Li_2S$ was produced in the final discharge process. The narrow pores of microporous carbon prevent the dissolution of polysulfides and influence the reaction mechanism of sulfur cathodes.

Received 28th September 2020
Accepted 26th October 2020

DOI: 10.1039/d0ra08299f

rsc.li/rsc-advances



## 1. Introduction

With the rapid development of electronic equipment and energy-storage devices, the demand for high-energy storage systems has become increasingly urgent and important. Sulfur cathodes have received much attention because of their high theoretical specific capacity (1672 mA h $g^{-1}$), low cost, high availability, and environment-friendliness.[1–4] Therefore, sulfur cathodes are considered as promising components of next-generation energy-storage systems.[5–8] However, current sulfur cathodes possess many disadvantages that prevent their rapid development. One of the most serious disadvantages is the high solubility of lithium polysulfides ($Li_2S_n$, $n = 4$–8) formed during the charging and discharging processes.[9–11] The dissolution of polysulfides leads to a low coulombic efficiency and rapid capacity degradation of batteries.[12–14]

Filling sulfur into microporous carbon is a promising method to overcome the dissolution problem caused by the high solubility of the polysulfide species in liquid electrolytes.[15–20] In the microporous carbon-supported sulfur cathode, the dissolution of polysulfides is suppressed because the solvent does not come into contact with sulfur.[21–23] Although this approach is effective in suppressing the polysulfide dissolution, the microporous carbon-supported sulfur cathodes show an electrochemical behavior different from that of their conventional sulfur counterparts, especially in the first discharge process.[15,17] The conventional sulfur cathode shows two plateaus at approximately 2.4 and 2.1 V *vs.* $Li/Li^+$ during the first discharge process.[11,16] During the first discharge plateau, the cyclic $S_8$ molecules are reduced to long-chain lithium polysulfides ($Li_2S_n$, $4 \leq n < 8$) through a disproportionation reaction, and the latter species are further reduced to short-chain lithium polysulfides ($Li_2S_n$, $1 < n < 4$) and $Li_2S$ during the second longer discharge plateau.[24–27] In contrast to the conventional sulfur cathode, the microporous carbon-supported sulfur cathode shows a single discharge plateau (~1.8 V *vs.* $Li/Li^+$) during the first discharge process.[15,18] To design a microporous carbon-supported sulfur cathode with high electrochemical performance, it is necessary to understand the reaction mechanism of the corresponding electrodes.

[a]*Graduate School of Human and Environmental Studies, Kyoto University, Yoshida-nihonmatsu-cho, Sakyo-ku, Kyoto 606-8501, Japan. E-mail: yamamoto.kentaro.4e@kyoto-u.ac.jp*

[b]*Department of Chemistry and Materials Engineering, Kansai University, 3-3-35 Yamate-cho, Suita, Osaka 564-8680, Japan*

[c]*Department of Mechanical Engineering, Kansai University, 3-3-35 Yamate-cho, Suita, Osaka 564-8680, Japan*

[d]*Institute of Advanced Sciences, Yokohama National University, 79-5 Tokiwadai, Hodogaya-ku, Yokohama 240-8501, Japan*

† Electronic supplementary information (ESI) available. See DOI: 10.1039/d0ra08299f

Various spectroscopic techniques such as X-ray photoemission spectroscopy (XPS)[28] and X-ray absorption spectroscopy[29] (XAS) have been employed to investigate the reaction mechanism of microporous carbon-supported sulfur cathodes. Helen *et al.* showed that on the surface and subsurface for the microporous carbon-supported sulfur cathode during first discharge by XPS, long-chain polysulfide could not be detected and only $Li_2S_2$ and $Li_2S$ could be detected.[28] They proposed a direct transformation from sulfur to $Li_2S_2$/$Li_2S$ during first discharge in the system.[28] On the other hand, Dominko *et al.* observed that a mixture of long chain polysulfide ($S_8^{2-}$ and $S_6^{2-}$) and a mixture of short chain polysulfides ($S_4^{2-}$ and $S_2^{2-}$) by *operando* XAS and suggested the transformation from the long-chain polysulfide to short-chain polysulfides and $Li_2S$.[29] However, thus far, no quantitative studies of the reaction mechanism have been reported. In this study, the reaction pathway of the microporous-supported sulfur cathodes was examined by the *operando* XAS analysis, which is a powerful technique to quantitatively evaluate the sulfur species formed during discharge/charge processes.[30,31]

## 2. Experimental

### 2.1 Materials

A microporous carbon-supported cathode was prepared using the procedure reported previously.[32] After mixing sulfur (Wako Co.) and microporous carbon (Toyobo Co.), the mixture was heated to 155 °C for approximately 5 h to allow sulfur to diffuse into the microporous carbon. Finally, the temperature was increased to 300 °C and maintained for 2 h to sublime the extra sulfur on the outer surface of the microporous carbon. Sulfur, $Li_2S_6$, $Na_2S_4$, $Na_2S_2$ and $Li_2S$ were used for the references of XAS. $Li_2S_6$ was synthesized through the previously reported procedure.[26] Stoichiometric ratio of sulfur and 1 M lithium triethylborohydride/tetrahydrofuran (3 : 1 mol%) was stirred for 1 hour and then the solvent was removed under vacuum inside Ar-filled glovebox. $Na_2S_4$ and $Na_2S_2$ were purchased from Dojindo Molecular Technologies Inc. Sulfur and $Li_2S$ were purchased from Aldrich Co.

### 2.2 Characterizations

The particle morphology of the microporous carbon was observed by transmission electron microscopy (TEM, JEM-2100F, JEOL) and scanning electron microscopy (SEM, SU-1500, Hitachi). The amount of sulfur in the microporous carbon was determined by thermogravimetric analysis (TGA) (DTG-60AH, Shimadzu) under an Ar atmosphere at a heating rate of 5 °C $min^{-1}$. $N_2$ adsorption and desorption isotherms were measured at −196 °C using Autosorbμ-iQ (Quantachrome).

### 2.3 Electrochemical testing

The electrochemical performance of the microporous carbon-supported sulfur cathode was examined using a two-electrode cell. A composite cathode was prepared by mixing the microporous carbon-supported sulfur cathode, acetylene black, and alginic acid binder in 90 : 5 : 5 weight ratio, supported by carbon paper. Li foil was used as the counter electrode. 1 M lithium bis(trifluorosulfonyl)amide (LiTFSA)/fluoroethylene carbonate (FEC):1,1,2,2-tetrafluoroethyl-2,2,3,3 tetrafluoropropyl ether (hydrofluoroether, HFE), in which the ratio of FEC to HFE was 1 : 1 vol% and the quantity of the electrolyte was 700 μL, was used as the electrolyte in a glass fiber membrane separator. The two-electrode cells were assembled in a glovebox filled with Ar. Galvanostatic charge/discharge measurements were carried out at a current density of 0.1 C (1 C = 1672 mA h $g^{-1}$) with cut-off voltages of 1.0 V for the discharge and 3.0 V for the charge process at 25 °C.

### 2.4 XAFS measurements

S K-edge *operando* XAS spectra of the microporous carbon-supported sulfur cathode were observed in the partial fluorescence yield (PFY) mode at the BL27SU beamline of the SPring-8 synchrotron radiation facility at Hyogo, Japan. A homemade cell[33] was used for the *operando* XAS. The microporous carbon-supported sulfur cathode composite material was mounted on a polyimide film to serve as the working electrode. LiTFSA/FEC:HFE was used in a glass fiber membrane as the electrolyte solution, and Li foil was used as the counter electrode. The *operando* cell was assembled in an argon-filled glovebox and transferred into a chamber for the XAS measurements under ultrahigh vacuum. The *operando* XAS measurements were performed under galvanostatic discharge at 0.1 C.

## 3. Results and discussion

The SEM and TEM images of microporous carbon are shown in Fig. 1a and b, respectively. The SEM image showed the particle size was 1–2 μm and the TEM image showed that the microporous carbon has amorphous structure with pore of ∼1 nm. The polar size distribution of the microporous carbon support was also confirmed by $N_2$ adsorption measurements, as shown in Fig. S1,† which showed a pore size of ∼1 nm. The TGA (Fig. S2†) showed a weight loss of approximately 24% at ∼450 °C for the microporous carbon-supported sulfur, indicating that the sulfur content was ∼24%.

The microporous carbon-supported sulfur cathode showed a discharge capacity of 2380 mA h $g^{-1}$, with a long single plateau at a voltage of ∼1.4 V in the first discharge process and a charge capacity of 900 mA h $g^{-1}$ (Fig. 2a). After the first discharge/charge cycle, the microporous carbon-supported sulfur cathode showed a different discharge curve, with a reversible capacity of 900 mA h $g^{-1}$ and a high coulombic efficiency (Fig. 2b). A large irreversible discharge capacity, exceeding the theoretical capacity of sulfur (1672 mA h $g^{-1}$), was also observed in previous reports.[17,21,28,32,34] This phenomenon is due to the formation of a solid electrolyte interphase (SEI) layer on the electrode composite.[23,35]

To examine the electronic structure of the pristine microporous-supported sulfur cathode, we performed *ex situ* S K-edge XAS measurements for the microporous carbon-supported sulfur and ring-like sulfur cathodes. The S K-edge XANES and EXAFS results are presented in Fig. 3a and b, respectively. The two sulfur samples showed an absorption

 

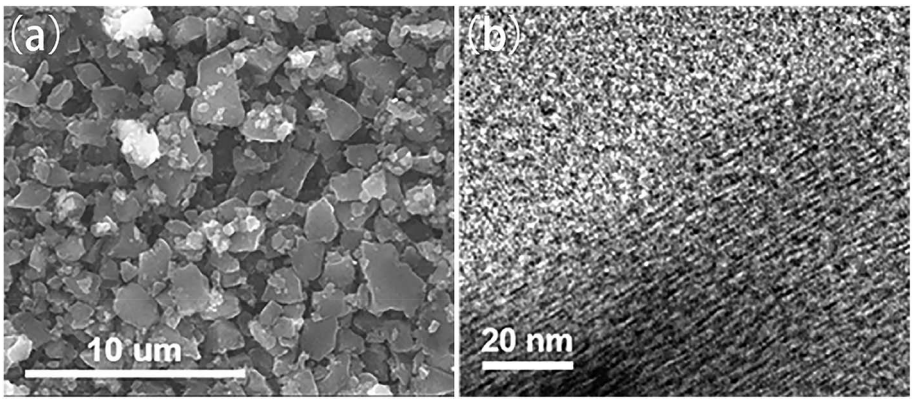


Fig. 1 (a) SEM and (b) TEM images of microporous carbon.

feature at 2471.8 eV, which was attributed to the S 1s to S–S $\pi^*$[36] state transition of elemental sulfur (Fig. 3a). However, the absorption peak intensity of the microporous carbon-supported sulfur cathode was lower than that of conventional sulfur, indicating that the transition from S 1s to S–S $\pi^*$ was reduced in the former sample. In the Fourier-transformed EXAFS spectra (Fig. 3b), the intensity of the peak at 1.6 Å, attributed to the S–S bonds, was lower for the microporous carbon-supported sulfur cathode than that for the conventional sulfur sample. This result indicates a decrease in the coordination number of S–S bonds in the microporous carbon-supported sulfur sample compared to that in conventional sulfur. Since sulfur in microporous carbons has been reported by X-ray photoemission spectroscopy[17] and electron energy loss spectroscopy[21] to be present in a chain rather than a ring structure, the present XAS results imply that sulfur changed from a ring to a chain structure after melting into the microporous carbon.

*Operando* XAS measurements were conducted to examine the electrochemical structural changes of the microporous carbon-supported sulfur cathode (Fig. 4a). Before the discharge process, absorption peaks were observed at 2472 and 2480 eV. The peak at 2472 eV is attributed to sulfur, as observed in Fig. 3, whereas that at 2480 eV corresponds to the sulfur component of the LiTFSA compound in the electrolyte.[25,37] During the discharge process, an absorption peak attributed to linear polysulfides appeared at 2470 eV;[36] then, two new peaks attributed to $Li_2S$ were observed at 2472.8 and 2475.2 eV.

Linear combination fitting (LCF)[26] was performed to estimate the ratio of the sulfur components during the discharge process (Fig. 4b). The spectra of pristine microporous carbon-supported sulfur $S_8$, long-chain polysulfides $S_6^{2-}$, medium/long-chain lithium polysulfides $S_4^{2-}$, short-chain polysulfides $S_2^{2-}$, and $Li_2S$ were used as references for the LCF analysis. The obtained fitting results were shown in Fig. S3.† Although these references were not exactly corresponding to polysulfide species forming during discharge process, they are useful to discuss the ratio change of polysulfide species.[25,26] The polysulfide species $S_6^{2-}$ and $S_2^{2-}$ were formed in the initial stage, with a corresponding decrease in the amount of $S_8$ species, whereas in the intermediate stage, the amounts of $S_2^{2-}$ and $Li_2S$ increased and those of $S_8$ and $S_6^{2-}$ decreased. In the final stage, the analysis showed an increase in the $Li_2S$ amount and a decrease in the amounts of $S_8$ and $S_2^{2-}$. Unreacted $S_8$ and $S_2^{2-}$ species were present even in the discharge state, that is, above the theoretical capacity of sulfur (1672 mA h $g^{-1}$).

The lithium content calculated by the LCF analysis (Fig. 4c) increased in the $x$ range of 0–3.0, but its value was lesser than that estimated by electrochemical measurements, and it was

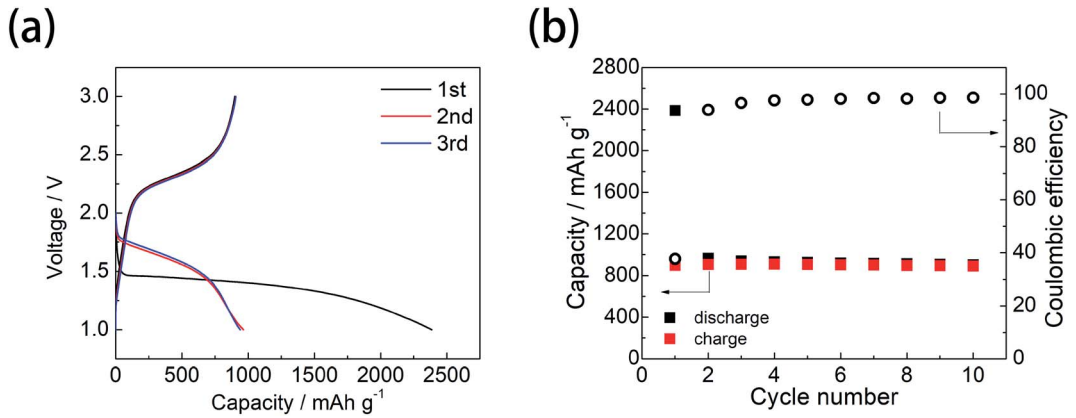


Fig. 2 Charge/discharge profile (a) and cycle performance (b) of the microporous carbon-supported sulfur cathode.

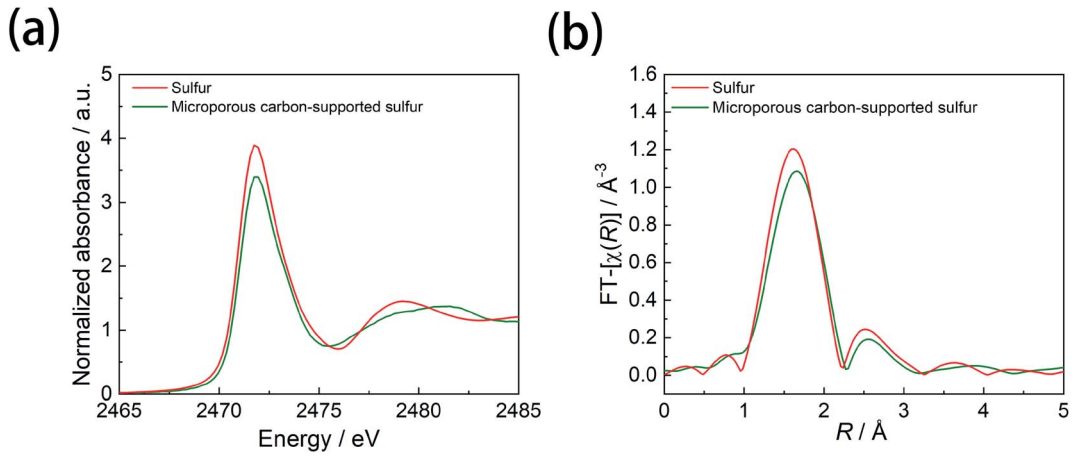


Fig. 3 (a) S K-edge XANES profiles and (b) S K-edge Fourier-transformed EXAFS profiles obtained from XAS measurements for sulfur and microporous carbon-supported sulfur cathodes.

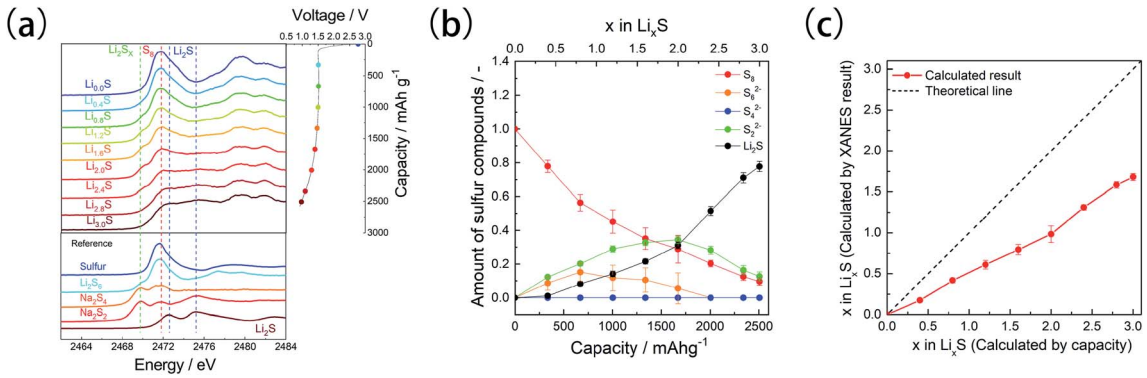


Fig. 4 (a) Sulfur K-edge XANES spectra obtained from the *operando* XAS measurements of the microporous carbon-supported sulfur cathode. (b) Sulfur compound ratio of the microporous carbon-supported sulfur cathode during the first discharge, calculated by the linear combination fitting (LCF) analysis of XANES spectra. (c) Lithium compositions calculated from the LCF analysis and electrochemical capacity data.

lesser than 2.0 even in the final discharge state ($x = 3.0$). These results indicate the decomposition of the electrolyte and the presence of unreacted sulfur species. It has been reported that the FEC solvent undergoes decomposition at 1.5 V (ref. 35) on the surface of the microporous carbon. In the microporous carbon-supported sulfur cathode, lithium-ion transport to the sulfur is sluggish compared to conventional sulfur cathode because the electrolyte cannot enter the micropores.[17] Therefore, lithium-ion conduction becomes the rate-limiting step, and the sulfur species located deep inside the micropores remain unreacted. A similar reaction distribution was observed in all-solid-state battery systems,[38] in which the reaction proceeds from the solid electrolyte side because ionic conduction is slower than electronic conduction.

The reaction mechanism of the microporous carbon-supported sulfur cathode during discharge is illustrated in

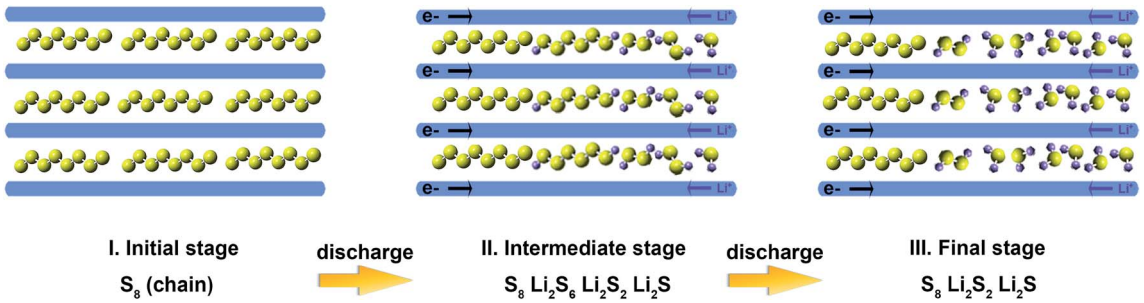


Fig. 5 Reaction model for the microporous carbon-supported sulfur cathodes.

 

Fig. 5. In the initial stage, sulfur forms chain structures inside the micropores. In the intermediate stage of discharge, $S_6^{2-}$ and $S_2^{2-}$ polysulfides are formed because the solvent cannot enter the micropores, and these polysulfides do not dissolve in the liquid electrolyte. In the final discharge process, $Li_2S$ is the main sulfide species, with residual amounts of $S_2^{2-}$ and long-chain $S_8$ species inside the micropores.

The microporous carbon can prevent the dissolution of polysulfides in the liquid electrolyte, resulting in a change in the sulfur cathode reaction pathway. This change leads to a single plateau at approximately 1.4 V during the first discharge, as observed in the solid electrolyte.

## 4. Conclusions

In this study, the reaction mechanism of the sulfur cathode in the microporous carbon during discharge was observed by *operando* XAS. The sulfur cathode was reduced to long-chain ($S_6^{2-}$) and short-chain ($S_2^{2-}$) polysulfide species during the initial discharge, while the short-chain $S_2^{2-}$ units were the main polysulfide species in the subsequent discharge; large amounts of $Li_2S$ were formed during the final discharge. The reaction mechanism of the microporous carbon-supported sulfur cathode is different from that of a conventional sulfur cathode, as the microporous carbon support prevents the dissolution of polysulfides. This study elucidated the reaction mechanism of sulfur cathodes in microporous carbon by *operando* soft XAS. We believe that our results can provide further insights into the deeper understanding of the behavior of sulfur in carbon-supported cathodes, and it will be helpful for designing new cathodes with high performance.

## Conflicts of interest

There are no conflicts to declare.

## Acknowledgements

This research was financially supported by the Japan Science and Technology Agency (JST), Advanced Low Carbon Technology Research and Development Program (ALCA), Specially Promoted Research for Innovative Next Generation Batteries (SPRING) Project (Grant Number: JPMJAL1301). Synchrotron radiation experiments were performed at beam line BL27SU of SPring-8 with the approval of the Japan Synchrotron Radiation Research Institute (JASRI) (Proposal number 2017A1025, 2017B1037, 2018A1025, 2018B1031, 2019A1021, 2019B1023, 2019B1634).

## Notes and references

1 G. Zhou, L.-C. Yin, D.-W. Wang, L. Li, S.-F. Pei, I. R. Gentle, F. Li and H.-M. Cheng, *ACS Nano*, 2013, **7**, 5367–5375.
2 B. L. Ellis, K. T. Lee and L. F. Nazar, *Chem. Mater.*, 2010, **22**, 691–714.
3 P. G. Bruce, S. A. Freunberger, L. J. Hardwick and J. M. Tarascon, *Nat. Mater.*, 2011, **11**, 19–29.
4 S. Evers and L. F. Nazar, *Acc. Chem. Res.*, 2013, **46**, 1135–1143.
5 Y.-X. Yin, S. Xin, Y.-G. Guo and L.-J. Wan, *Angew. Chem., Int. Ed.*, 2013, **52**, 13186–13200.
6 A. Manthiram, Y. Fu, S.-H. Chung, C. Zu and Y.-S. Su, *Chem. Rev.*, 2014, **114**, 11751–11787.
7 Q. Pang, X. Liang, C. Y. Kwok and L. F. Nazar, *Nat. Energy*, 2016, **1**, 16132.
8 Z. W. Seh, Y. Sun, Q. Zhang and Y. Cui, *Chem. Soc. Rev.*, 2016, **45**, 5605–5634.
9 M. Vijayakumar, N. Govind, E. Walter, S. D. Burton, A. Shukla, A. Devaraj, J. Xiao, J. Liu, C. Wang, A. Karim and S. Thevuthasan, *Phys. Chem. Chem. Phys.*, 2014, **16**, 10923–10932.
10 S. S. Zhang, *J. Power Sources*, 2013, **231**, 153–162.
11 Z. Lin and C. Liang, *J. Mater. Chem. A*, 2015, **3**, 936–958.
12 G. Y. Zheng, Y. Yang, J. J. Cha, S. S. Hong and Y. Cui, *Nano Lett.*, 2011, **11**, 4462–4467.
13 X. L. Ji and L. F. Nazar, *J. Mater. Chem.*, 2010, **20**, 9821–9826.
14 X. L. Ji, S. Evers, R. Black and L. F. Nazar, *Nat. Commun.*, 2011, **2**, 325.
15 B. Zhang, X. Qin, G. R. Li and X. P. Gao, *Energy Environ. Sci.*, 2010, **3**, 1531–1537.
16 S. Xin, L. Gu, N. H. Zhao, Y. X. Yin, L. J. Zhou, Y. G. Guo and L. J. Wan, *J. Am. Chem. Soc.*, 2012, **134**, 18510–18513.
17 Z. Li, L. X. Yuan, Z. Q. Yi, Y. M. Sun, Y. Liu, Y. Jiang, Y. Shen, Y. Xin, Z. L. Zhang and Y. H. Huang, *Adv. Energy Mater.*, 2014, **4**, 1301473.
18 Z. Li, Y. Jiang, L. X. Yuan, Z. Q. Yi, C. Wu, Y. Liu, P. Strasser and Y. H. Huang, *ACS Nano*, 2014, **8**, 9295–9303.
19 Z. H. Peng, W. Y. Fang, H. B. Zhao, J. H. Fang, H. W. Cheng, T. N. L. Doan, J. Q. Xu and P. Chen, *J. Power Sources*, 2015, **282**, 70–78.
20 Y. H. Xu, Y. Wen, Y. J. Zhu, K. Gaskell, K. A. Cychosz, B. Eichhorn, K. Xu and C. S. Wang, *Adv. Funct. Mater.*, 2015, **25**, 4312–4320.
21 M. Helen, T. Diemant, S. Schindler, R. J. Behm, M. Danzer, U. Kaiser, M. Fichtner and M. A. Reddy, *ACS Omega*, 2018, **3**, 11290–11299.
22 S. Z. Niu, G. M. Zhou, W. Lv, H. F. Shi, C. Luo, Y. B. He, B. H. Li, Q. H. Yang and F. Y. Kang, *Carbon*, 2016, **109**, 1–6.
23 E. Markevich, G. Salitra, A. Rosenman, Y. Talyosef, F. Chesneau and D. Aurbach, *J. Mater. Chem. A*, 2015, **3**, 19873–19883.
24 D. Zheng, G. Wang, D. Liu, J. Si, T. Ding, D. Qu, X. Yang and D. Qu, *Adv. Mater. Technol.*, 2018, **3**, 1700233.
25 M. Cuisinier, P.-E. Cabelguen, S. Evers, G. He, M. Kolbeck, A. Garsuch, T. Bolin, M. Balasubramanian and L. F. Nazar, *J. Phys. Chem. Lett.*, 2013, **4**, 3227–3232.
26 M. Cuisinier, C. Hart, M. Balasubramanian, A. Garsuch and L. F. Nazar, *Adv. Energy Mater.*, 2015, **5**, 1401801.
27 G. R. Li, S. Wang, Y. N. Zhang, M. Li, Z. W. Chen and J. Lu, *Adv. Mater.*, 2018, **30**, 1705590.
28 M. Helen, M. A. Reddy, T. Diemant, U. Golla-Schindler, R. J. Behm, U. Kaiser and M. Fichtner, *Sci. Rep.*, 2015, **5**, 12146.

29 R. Dominko, A. Vizintin, G. Aquilanti, L. Stievano, M. J. Helen, A. R. Munnangi, M. Fichtner and I. Arcon, *J. Electrochem. Soc.*, 2018, **165**, A5014–A5019.
30 R. Xu, J. Lu and K. Amine, *Adv. Energy Mater.*, 2015, **5**, 1500408.
31 L. Zhang, T. Qian, X. Y. Zhu, Z. L. Hu, M. F. Wang, L. Y. Zhang, T. Jiang, J. H. Tian and C. L. Yan, *Chem. Soc. Rev.*, 2019, **48**, 5432–5453.
32 T. Takahashi, M. Yamagata and M. Ishikawa, *Prog. Nat. Sci.: Mater. Int.*, 2015, **25**, 612–621.
33 K. Yamamoto, Y. Y. Zhou, N. Yabuuchi, K. Nakanishi, T. Yoshinari, T. Kobayashi, Y. Kobayashi, R. Yamamoto, A. Watanabe, Y. Orikasa, K. Tsuruta, J. Park, H. R. Byon, Y. Tamenori, T. Ohta and Y. Uchimoto, *Chem. Mater.*, 2020, **32**, 139–147.
34 W. H. Zhang, D. Qiao, J. X. Pan, Y. L. Cao, H. X. Yang and X. P. Ai, *Electrochim. Acta*, 2013, **87**, 497–502.
35 E. Markevich, G. Salitra, A. Rosenman, Y. Talyosef, F. Chesneau and D. Aurbach, *Electrochem. Commun.*, 2015, **60**, 42–46.
36 X. Li, M. Banis, A. Lushington, X. F. Yang, Q. Sun, Y. Zhao, C. Q. Liu, Q. Z. Li, B. Q. Wang, W. Xiao, C. H. Wang, M. S. Li, J. W. Liang, R. Y. Li, Y. F. Hu, L. Goncharova, H. M. Zhang, T. K. Sham and X. L. Sun, *Nat. Commun.*, 2018, **9**, 4509.
37 C. W. Lee, Q. Pang, S. Ha, L. Cheng, S. D. Han, K. R. Zavadil, K. G. Gallagher, L. F. Nazar and M. Balasubramanian, *ACS Cent. Sci.*, 2017, **3**, 605–613.
38 K. Chen, S. Shinjo, A. Sakuda, K. Yamamoto, T. Uchiyama, K. Kuratani, T. Takeuchi, Y. Orikasa, A. Hayashi, M. Tatsumisago, Y. Kimura, T. Nakamura, K. Amezawa and Y. Uchimoto, *J. Phys. Chem. C*, 2019, **123**, 3292–3298.